



HAL
open science

Overexpression of MLN51 triggers P-body disassembly and formation of a new type of RNA granules

N. Cougot, E. Daguinet, A. Baguet, A. Cavalier, D. Thomas, P. Bellaud, A. Fautrel, F. Godey, Edouard Bertrand, C. Tomasetto, et al.

► **To cite this version:**

N. Cougot, E. Daguinet, A. Baguet, A. Cavalier, D. Thomas, et al.. Overexpression of MLN51 triggers P-body disassembly and formation of a new type of RNA granules. *Journal of Cell Science*, 2014, 127 (21), pp.4692–701. 10.1242/jcs.154500 . hal-02191565

HAL Id: hal-02191565

<https://hal.science/hal-02191565>

Submitted on 1 Jun 2021

HAL is a multi-disciplinary open access archive for the deposit and dissemination of scientific research documents, whether they are published or not. The documents may come from teaching and research institutions in France or abroad, or from public or private research centers.

L'archive ouverte pluridisciplinaire **HAL**, est destinée au dépôt et à la diffusion de documents scientifiques de niveau recherche, publiés ou non, émanant des établissements d'enseignement et de recherche français ou étrangers, des laboratoires publics ou privés.

RESEARCH ARTICLE

Overexpression of MLN51 triggers P-body disassembly and formation of a new type of RNA granules

Nicolas Cougot¹, Élisabeth Dagueneau², Aurélie Baguet², Annie Cavalier¹, Daniel Thomas¹, Pascale Bellaud³, Alain Fautrel³, Florence Godey⁴, Édouard Bertrand^{5,*}, Catherine Tomassetto^{2,*} and Reynald Gillet^{1,*}

ABSTRACT

Metastatic lymph node 51 (MLN51, also known as CASC3) is a core component of the exon junction complex (EJC), which is loaded onto spliced mRNAs and plays an essential role in determining their fate. Unlike the three other EJC core components [eIF4AIII, Magoh and Y14 (also known as RBM8A)], MLN51 is mainly located in the cytoplasm, where it plays a key role in the assembly of stress granules. In this study, we further investigated the cytoplasmic role of MLN51. We show that MLN51 is a new component of processing bodies (P-bodies). When overexpressed, MLN51 localizes in novel small cytoplasmic foci. These contain RNA, show directed movements and are distinct from stress granules and P-bodies. The appearance of these foci correlates with the process of P-body disassembly. A similar reduction in P-body count is also observed in human HER2-positive (HER2⁺) breast cancer cells overexpressing MLN51. This suggests that P-body disassembly and subsequent mRNA deregulation might correlate with cancer progression.

KEY WORDS: Breast cancer, mRNA, MLN51, P-bodies, Stress granules

INTRODUCTION

MLN51 (metastatic lymph node 51, also known as CASC3) is a protein involved in mRNA metabolism through its association with the exon junction complex (EJC). The EJC is a macromolecular complex that is deposited by the splicing machinery onto mRNAs at the exon–exon junction. EJC binding is a crucial step in determining the subsequent fate of mRNA, as the EJC has been proposed to regulate pre-mRNA splicing, cytoplasmic export, localization, translation and transcript stability (Degot et al., 2004; Nott et al., 2004; Palacios et al., 2004; Gehring et al., 2005; Tange et al., 2005). The N-terminal region of MLN51 harbors the speckle localizer and RNA-binding module (SELOR), a unique RNA-binding domain that triggers the incorporation of MLN51 into the exon junction complex core (Degot et al., 2004; Ballut et al., 2005).

The C-terminal moiety of MLN51 contains a nuclear export signal that allows the protein to shuttle between the nucleus and the cytoplasm and, interestingly, it is this particular region that is essential for the recruitment of MLN51 to cytoplasmic stress granules (Baguet et al., 2007).

Stress granules self-assemble in response to a wide variety of environmental stresses that can cause general translational arrest (Anderson and Kedersha, 2006). Several factors involved in translation, mRNA decay or mRNA silencing have been found to localize in stress granules (Kedersha and Anderson, 2007), leading to the description of stress granules as cytoplasmic compartments involved in the remodeling of messenger ribonucleoprotein particles (Mollet et al., 2008). They share some components with other non-membranous cytoplasmic structures called processing bodies (P-bodies) that are involved in mRNA storage, translational repression and decay (Eystathiou et al., 2002; Sheth and Parker, 2003; Cougot et al., 2004; Pillai et al., 2005; Eulalio et al., 2007; Parker and Sheth, 2007). Recently, we deciphered the structural organization of P-bodies and showed that they are organized into two compartments – a dense central core containing mRNA decay factors and a peripheral shell enriched with polysomes and translational activators (Cougot et al., 2012; Cougot et al., 2013). Overall, the presence of these two cytoplasmic substructures fits the ‘mRNA cycle’ model, according to which cytoplasmic mRNAs cycle between active polysomes, P-bodies and stress granules (Balagopal and Parker, 2009).

Because MLN51 was recently shown to be a translational activator and to be present in active polysomes (Chazal et al., 2013), we investigated the involvement of MLN51 in the mRNA cycle and explored the role of this protein in stress granules and P-bodies in HeLa and malignant breast cancer cells. In the present study, we show that endogenous MLN51 is a novel component of P-bodies. When overexpressed, it accumulates in two types of cytoplasmic foci – in stress granules and in a novel mRNA-containing granular structure that we named SMIGs (small MLN51-induced granules). These newly described cytoplasmic bodies contain RNAs and show directed movements. Moreover, MLN51 overexpression leads to microtubule-dependent P-body disassembly. Interestingly, a similar reduction in P-body count and MLN51 localization in small granules is also observed in human HER2⁺ breast cancer cells overexpressing MLN51, suggesting that P-body disassembly and subsequent mRNA deregulation might be linked to certain cancers.

RESULTS**Endogenous MLN51 is a novel component of P-bodies**

To better characterize the cytoplasmic pattern of MLN51 distribution, we raised polyclonal antibodies directed against

¹Université de Rennes 1, UMR CNRS 6290 IGDR, «Translation and Folding Team», Campus de Beaulieu, 35042 Rennes cedex, France. ²Institut de Génétique et de Biologie Moléculaire et Cellulaire, UMR 7104, CNRS/U964 INSERM/Université de Strasbourg, 67404 Illkirch, France. ³Unité INSERM 991, Plateforme histopathologique, IFR 140 GFAS, Université de Rennes 1, 35043 Rennes, France. ⁴Centre de Ressources Biologiques Santé de Rennes, Centre Eugène Marquis, Rue de la Bataille Flandres Dunkerque – 35042 Rennes cedex, France. ⁵Institut de Génétique Moléculaire de Montpellier, CNRS, UMR 5535, 34293 Montpellier cedex 5, France.

*Authors for correspondence (edouard.bertrand@igmm.cnrs.fr; cat@igbmc.fr; reynald.gillet@univ-rennes1.fr)

the N-terminal part of the protein (Degot et al., 2002). MLN51 was first detected by immunofluorescence in HeLa cells, which were also immunolabelled with antibodies against Ge1 (also known as EDC4) or human Dcp1a that allow detection of P-bodies (Kedersha and Anderson, 2007) (Fig. 1A,B). We observed that endogenous MLN51 accumulated in cytoplasmic foci that colocalized with both P-bodies markers. MLN51 is, in fact, the first member of the EJC core to be detected in P-bodies. To more precisely assess its localization, we performed immunoelectron microscopy using the same antibodies (Fig. 1C). MLN51-labeling gold particles were enriched by a factor of 48.47 in the P-bodies compared to the surrounding cytoplasm – 1990.54 ± 1354.16 gold particles/ μm^2 (mean \pm s.d.) inside the P-bodies ($n=11$) and 41.07 ± 17.04 gold particles/ μm^2 outside. Quantification of the gold-labeling in the P-bodies was performed in an internal P-body area that was calculated by a 50% downscaling of the external contour added to the peripheral zone between it and the entire electron-dense body (Cougot et al., 2012). The peripheral and internal areas correspond to 75% and 25% of the total area, respectively. About 75% of the MLN51-labeling gold particles accumulated at the periphery of mammalian P-bodies (604 of the 806 gold-particles counted on 11 different hDcp1a gold-labeled P-bodies). Collectively, these results show that MLN51 is distributed equally throughout the granule.

Overexpression of MLN51 leads to P-body disassembly

We next analyzed the effects of MLN51 overexpression on P-bodies. To do so, CFP–MLN51 was expressed in HeLa cells, and we performed co-labeling of P-bodies using an anti-Dcp1a antibody (Fig. 2A). Surprisingly, MLN51-overexpressing cells showed a reduced number of P-bodies compared with that of untransfected cells, even though the levels of endogenous Dcp1a are not affected by MLN51 overexpression (Fig. 2B). P-body disassembly following MLN51 overexpression was confirmed when using various P-body markers, such as Dcp1, Ge1, rck/p54

or Xrn1 (Fig. 2C). We performed quantitative analysis and observed a 1.9-fold decrease in the number of cells containing at least one P-body (29 out of 54 transfected cells with at least one P-body, Fig. 3C,D). The average number of P-bodies per cell was decreased by a factor of 3.5 (2.66 P-bodies per cell in untransfected cells versus 0.76 in cells overexpressing CFP–MLN51), and the distribution of the number of P-bodies per cell showed a shift towards cells having fewer P-bodies, with a strong increase in the number of cells having zero or one. In fact, after MLN51 overexpression, 88% of the cells had less than one P-body, whereas this was the case in only 5.7% of untransfected cells (Fig. 2D).

P-body disassembly is not linked to the role of MLN51 in the EJC

We wanted to explore whether the effect of MLN51 overexpression on P-bodies is linked to the role of MLN51 in the EJC. MLN51 is composed of two domains (Fig. 3A): (1) the N-terminal domain contains a nuclear localization signal and is involved in the recruitment of MLN51 to the EJC core through the SELOR domain (Degot et al., 2004; Ballut et al., 2005) and (2) the C-terminal domain contains a nuclear export signal and plays a role in the recruitment of the protein to cytoplasmic stress granules (Baguet et al., 2007). First, we confirmed by western blot experiments that overexpression of MLN51 fragments had no effect on the level of expression of endogenous p54 and Dcp1a (Fig. 3B). Then, we observed that overexpression of the MLN51 N-terminus or SELOR did not have a significant effect on P-body number, irrespective of the P-body marker examined [hDcp1 (Fig. 3C) or p54 (Fig. 3D)]. The overexpression of the MLN51 C-terminal fragment induced a similar phenotype to that of the full-length protein (Fig. 3C,D). Taken together, these results suggest that the effect of MLN51 on P-body number is not linked to its association with the EJC. To confirm this, we overexpressed a mutant of MLN51 (H220A/D221A, MLN51HD) that has previously been shown to prevent MLN51 incorporation into

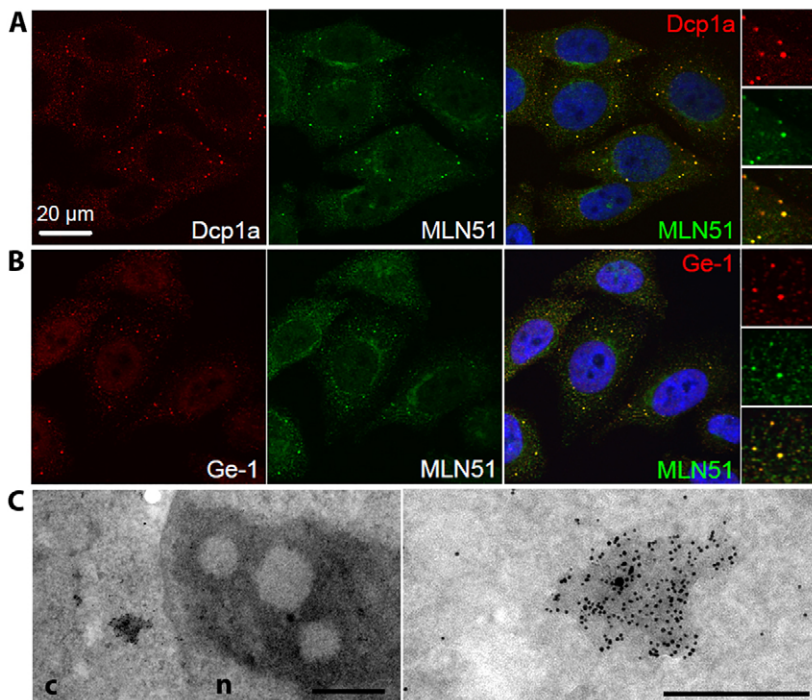


Fig. 1. Endogenous MLN51 is a novel component of mammalian P-bodies. Human Dcp1a, detected with anti-Dcp1a (A, left panel, red) or human Ge1, detected with anti-Ge1 (B, left panel, red) and endogenous MLN51, detected with rabbit anti-MLN51 (A,B, central panel, green), colocalize in the P-body. Cy3 and FITC overlays are shown in the right column, with DAPI-stained nuclei (blue). Scale bar: 20 μm . (C) MLN51 (6-nm gold particles) is localized throughout the P-body, which is labeled with anti-Dcp1a (15-nm gold particles) in high-pressure frozen and chemical-embedded HeLa cells. n, nucleus; c, cytoplasm. Scale bars: 500 nm (left panel), 100 nm (right panel).

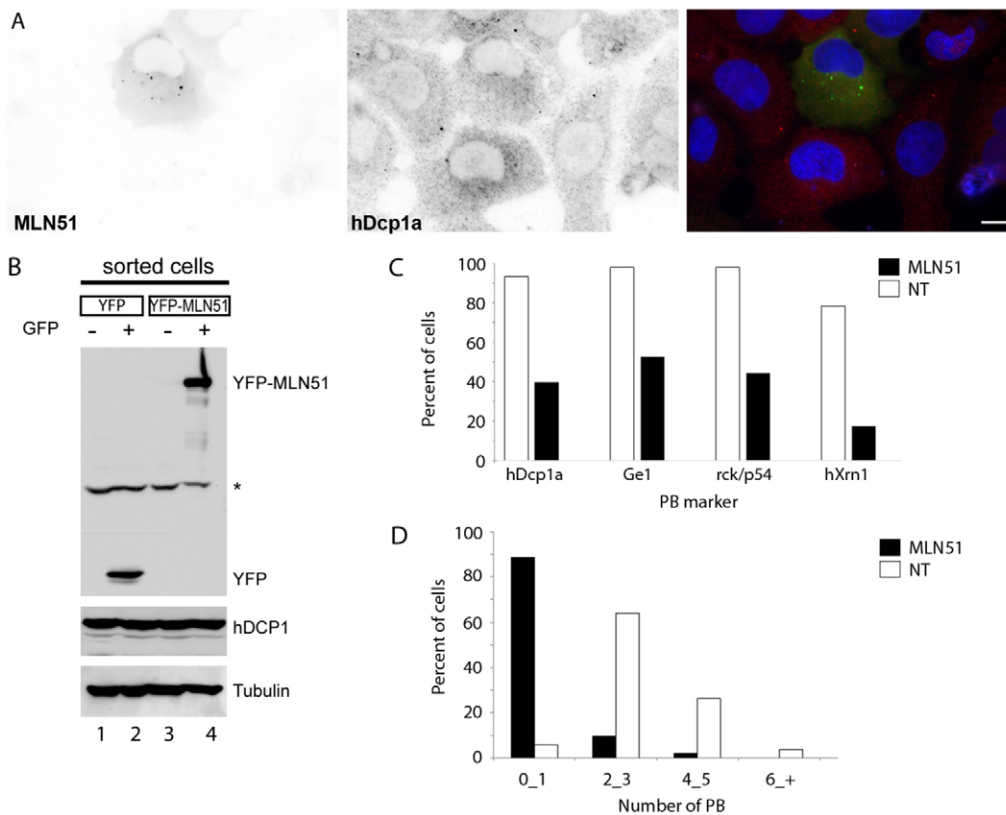


Fig. 2. Overexpression of MLN51 induces P-body disassembly.

(A) HeLa cells overexpressing CFP–MLN51 (left panel, green) have no P-bodies detected with anti-Dcp1a (central panel, red). Scale bar: 20 μ m. (B) Overexpression of MLN51 has no effect on the level of endogenous Dcp1a. HeLa cells transfected with YFP alone (lanes 1,2) and YFP–MLN51 (lanes 3,4) were separated by fluorescence-activated cell sorting into two distinct populations, one negative for YFP (–) and the other positive for YFP (+). Sorted populations were analyzed by western blotting using antibodies against GFP, p54, Dcp1a and tubulin. The asterisk represents a non-specific signal. (C) Graph showing the percentage of cells having at least one P-body (PB) following overexpression of CFP–MLN51. P-body disassembly following overexpression of MLN51 is observed with various P-body markers. P-bodies were counted following immunodetection with antibodies against Dcp1a, Ge1, p54 and hXrn1. (D) Distribution of the number of P-bodies per cell following overexpression of CFP–MLN51 (as determined by immunodetection with anti-Dcp1a). NT, untransfected cells.

EJCs both *in vitro* and *in vivo* (Ballut et al., 2005; Daguinet et al., 2012). As shown in Fig. 3C,D, overexpression of this mutant led to the disassembly of P-bodies (~40% of the cells overexpressing MLN51HD contained at least one PB). Finally, we overexpressed two other core EJC components, eIF4A3 and Y14, and no significant effect on P-bodies was noticed (supplementary material Fig. S1). Similar observations were made with other P-body markers (Ge1, Xrn1).

Overexpression of MLN51 leads to its accumulation in SMIGs

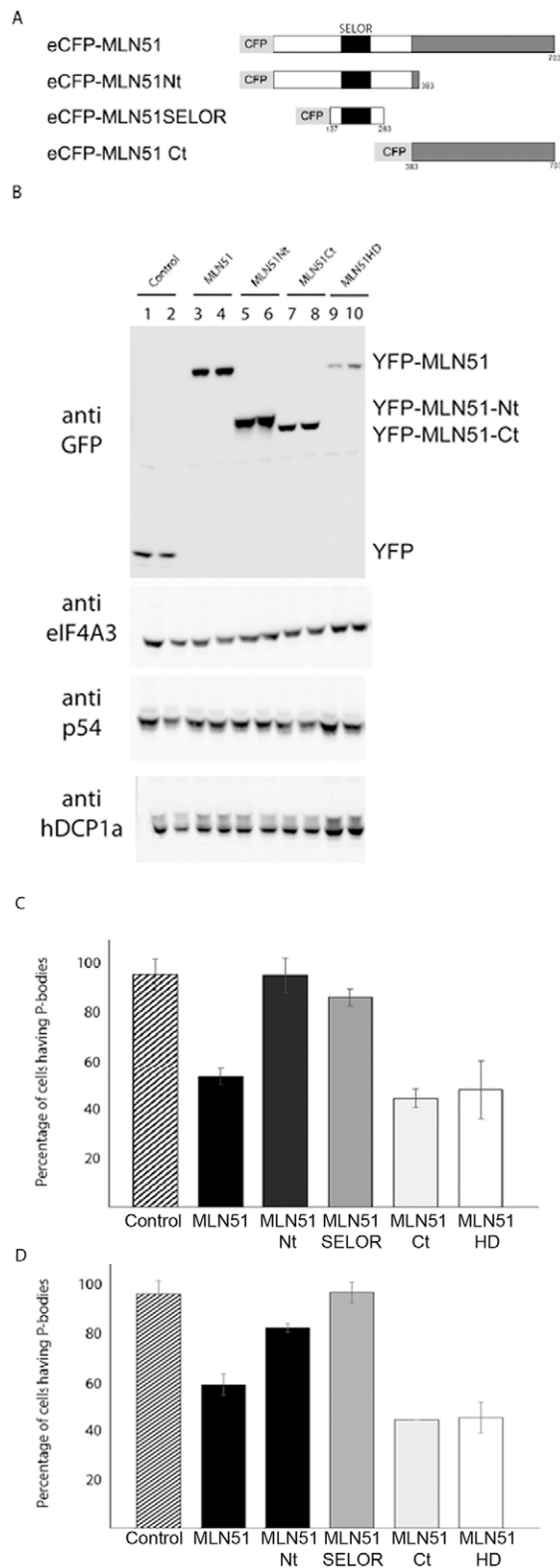
Unlike the three other core EJC components (eIF4AIII, Magoh and Y14), MLN51 is primarily found in the cytoplasm, and we observed that the protein is present in P-bodies. As previously reported (Baguet et al., 2007), we confirmed the distribution of overexpressed MLN51 into three cytoplasmic fractions – diffuse (18.5%), small foci (77.8%) and larger foci (3.7%) (Fig. 2; Fig. 4C). Given that MLN51 is a stress granule component and participates in stress granule assembly, we wondered whether these foci could be related to stress granules. To better identify the cytoplasmic structures, we transiently expressed a CFP-tagged version of MLN51 in HeLa cells, then performed a series of co-stainings using antibodies against three stress granule markers – TIA1, FMRP and PABP (Buchan and Parker, 2009). Interestingly, we observed that the small MLN51 foci were negative for TIA1, FMRP and PABP markers (Fig. 4). Given that the larger foci did colocalize with all of these stress granule components (supplementary material Fig. S2A–C), this suggests that only the larger foci are stress-granule-related; the small foci correspond to unknown granules that we named ‘small MLN51-induced granules (SMIGs)’. It is important to note that the appearance of SMIGs is associated only with the expression of

full-length MLN51, whereas the larger foci can also be observed following the overexpression of the MLN51 C-terminal domain.

SMIGs are mobile RNA granules

To further characterize SMIGs, we analyzed whether these granules contained RNA. Poly(A)⁺ mRNAs were detected by *in situ* hybridization using Cy5-labeled oligo d(T) probes in HeLa cells overexpressing CFP–MLN51. Triple fluorescence labeling experiments were then performed in order to determine the colocalization of MLN51, poly(A)⁺ and ATXN2, a component of stress granules. We found that poly(A)⁺ mRNAs actually colocalized with MLN51 and ATXN2 in stress granules (Fig. 5A) and only with MLN51 in SMIGs (Fig. 5B). Co-staining experiments of SMIGs with antibodies directed against the nuclear form of PABP and against the nuclear cap-binding protein CBP80 (also known as NCBP1) were performed, in order to determine whether mRNAs in SMIGs have actually been translated. However, SMIGs were negative for these both markers (supplementary material Fig. S3).

Thus, one possibility was that a SMIG is a precursor to a stress granule. To address this, we first studied the dynamics of these two types of granules. We performed time-lapse live-cell imaging on cells overexpressing CFP–MLN51, taking one picture every 0.5 seconds over 5 minutes (Fig. 6A; supplementary material Movie 1). We observed that, contrary to the MLN51-containing stress granules that did not move, SMIGs showed directed movements. Calculation of the mean squared displacement was performed on 119 SMIGs, and this showed that, when mobile, SMIGs show directed movements with an average speed of 3.7 μ m/s over an average distance of 4 μ m (Fig. 6B). It has been shown previously that microtubules are required for stress granule



assembly (Ivanov et al., 2003). As SMIGs show directed movements, it would be tempting to hypothesize that these movements are involved in subsequent stress granule assembly. To test this hypothesis, we investigated the effects of microtubule disassembly on MLN51 localization and dynamics. At 24 hours

Fig. 3. P-body disassembly is independent of MLN51 function in the EJC. (A) Schematic representation of the different MLN51 constructs used in this study. HeLa cells were transfected with MLN51, MLN51 N-terminus (Nt), MLN51 SELOR, MLN51 C-terminus (Ct) or MLN51HD, fused to either YFP or CFP. P-bodies were detected by immunofluorescence with the anti-Dcp1a antibody. (B) Overexpression of MLN51 fragments has no effect on the level of expression of endogenous p54 and Dcp1a. HeLa cells were transfected with YFP alone (lanes 1,2), YFP–MLN51 (lanes 3,4), YFP–MLN51 N-terminus (lanes 5,6), YFP–MLN51 C-terminus (lanes 7,8) or YFP–MLN51HD (lanes 9,10) and analyzed by western blotting using antibodies against GFP, p54, Dcp1a and eIF4A3 antibodies. (C,D) Graphs of the percentage of cells having at least one P-body following overexpression of CFP fusions of full-length MLN51 (MLN51), MLN51 N-terminus, MLN51 SELOR domain, MLN51 C-terminus or the MLN51HD mutant. P-bodies are detected with the anti-Dcp1a antibody (C) or p54 antibody (D). Data show the mean \pm s.d.

after transfection, cells expressing the full-length CFP–MLN51 protein were treated for 2 hours with nocodazole, an antimicrotubule agent known to alter microtubule assembly. Although we found that, following treatment, the number of cells containing SMIGs decreased from 77.8% to 46.2% – similar to results that have been described previously for stress granules (Ivanov et al., 2003) – live-cell imaging failed to show any sort of SMIG fusion as a prerequisite for stress granule formation (data not shown). Taken together, our results reinforce the notion that the SMIGs are certainly distinct cytoplasmic entities rather than nascent stress granules.

We next wanted to see whether the P-body count was microtubule dependent. HeLa cells were transfected with CFP–MLN51. After 24 hours of expression, cells were treated for 2 hours with nocodazole and P-bodies were detected with anti-Dcp1a. As already established (Sweet et al., 2007; Aizer et al., 2008), nocodazole treatment increases the number of P-bodies by a factor of 3 – 8.23 P-bodies per cell following nocodazole treatment ($n=55$) versus 2.66 P-bodies per cell ($n=53$) in untransfected cells. It also strikingly reduces the effect of MLN51 overexpression on the number of P-bodies. Following nocodazole treatment, the average number of P-bodies per cell was reduced by a factor of 1.5 compared with the 3.5-fold reduction observed in untreated cells, and the percentage of cells having P-bodies is similar to that of untransfected cells. Interestingly, after nocodazole treatment, we observed a fourfold increase in contacts between SMIG and P-body markers (27% formed contacts in nocodazole-treated cells versus 7% in untreated cells). Taken together, these results suggest that overexpression of MLN51 induces the disassembly of P-bodies in a microtubule-dependent manner.

P-body disassembly is observed in HER2⁺ breast cancer cells that overexpress MLN51

In 50% of HER2⁺ breast cancers, *MLN51* is co-amplified with *c-ErbB2* (the gene encoding HER2) and the other genes of the amplicon (Bièche et al., 1996; Degot et al., 2002; Arriola et al., 2008). We analyzed the number of P-bodies in HER2⁺ breast cancer cells that either did or did not overexpress MLN51 [HER2⁺/MLN51⁺ (patient 204817) and HER2⁺/MLN51⁻ (patient 20416E), respectively]. We compared this with the number of P-bodies in normal breast cells (patient P12/28 821) and HER2-negative cells [HER2⁻/MLN51⁻, a breast tumor with a HER2 immunohistochemistry (IHC) score of 0 (patient 207861)]. Overexpression of MLN51 was assessed by immunofluorescence (Fig. 7) and by IHC (supplementary

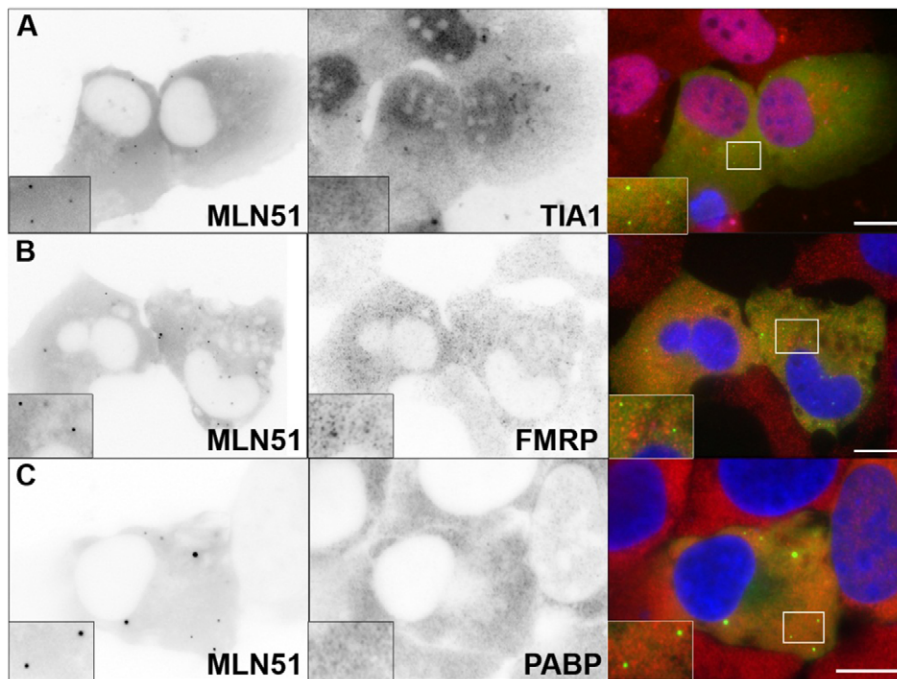


Fig. 4. MLN51 accumulates in SMIGs that are not stress granules. Cells were transfected with CFP–MLN51 (left column, green in right column). Stress granules were immunodetected with antibodies against TIA1 (A), FMRP (B) and PABP (C) (central column, red in right column). Right column shows overlay of left and central panels with DAPI-stained nuclei. Insets show granule enlargements from the areas indicated in the images on the right. Scale bars: 10 μ m.

material Fig. S4). P-bodies were counted following detection by immunofluorescence using anti-Dcp1a antibodies (Fig. 7). For $HER2^+/MLN51^+$ samples, we focused on cells that showed higher levels of overexpression of MLN51 (128 of 1380 cells; Fig. 7D; supplementary material Fig. S4D). Noticeably, in agreement with our observation in HeLa cells, the average number of P-bodies per cell was decreased in $HER2^+$ breast cancer cells overexpressing MLN51 as compared with that of normal breast cells [2.08 P-bodies per cell in $HER2^+/MLN51^+$ cells ($n=128$) versus 3.53 P-bodies per cell in normal cells ($n=1299$)]. It was also decreased when compared with the number in $HER2^+$ breast cancer cells that did not overexpress MLN51 [3.7 P-bodies per cell ($n=910$)]. And finally, it decreased when compared with the number of P-bodies in $HER2^-$ cells

[3.99 P-bodies per cell in $HER2^-/MLN^-$ ($n=1103$)]. The percentage of cells containing less than one P-body is strongly increased in $HER2^+/MLN51^+$ samples (43% compared with 18% in normal breast cells), whereas the percentage of cells with more than six P-bodies was decreased in the $HER2^+/MLN51^+$ sample versus the normal sample (2% compared with 19%). Finally, overexpression of MLN51 resulted in its localization into small cytoplasmic granules that resemble SMIGs (Fig. 7D, inset). Breast cancer cells that do not overexpress MLN51 show a similar distribution of P-body number to that found in normal breast cells (Fig. 7E). These results show that, in $HER2^+$ breast cancer cells that overexpress MLN51, the number of P-bodies is reduced in a similar manner to that observed after overexpression of MLN51 in HeLa cells.

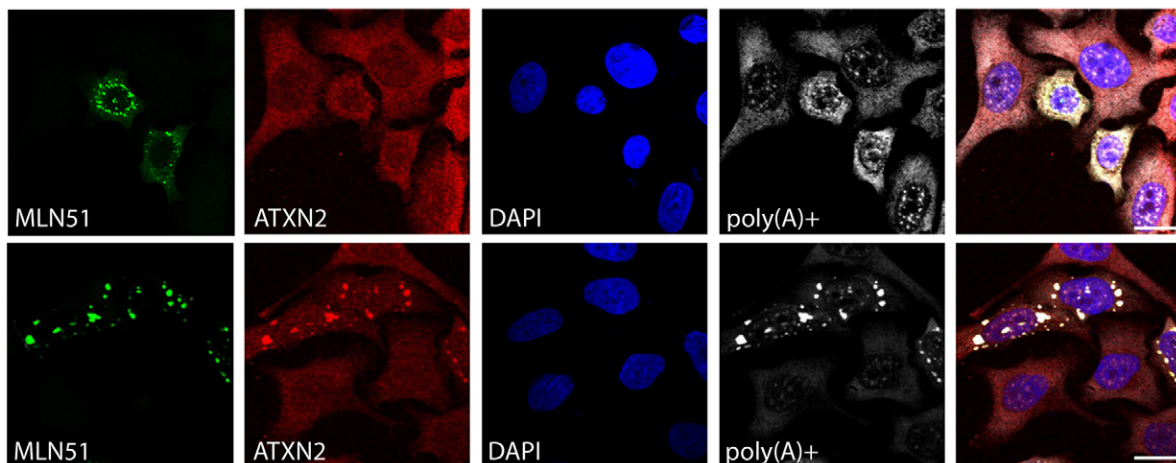


Fig. 5. SMIGs contain poly(A)⁺ RNA. CFP–MLN51 (left panels, green) was transfected in HeLa cells. At 24 hours following transfection, poly(A)⁺ mRNA (fourth panels, white) was detected by fluorescence *in situ* hybridization with a Cy5-labeled oligo d(T) probe, stress granules (second panels, red) were detected with the anti-ATXN2 antibody. DNA is stained with DAPI (blue) (A) SMIGs contain poly(A)⁺ mRNA but no stress granule markers. (B) Stress granules contain ATXN2 and poly(A)⁺ mRNAs. Scale bars: 10 μ m.

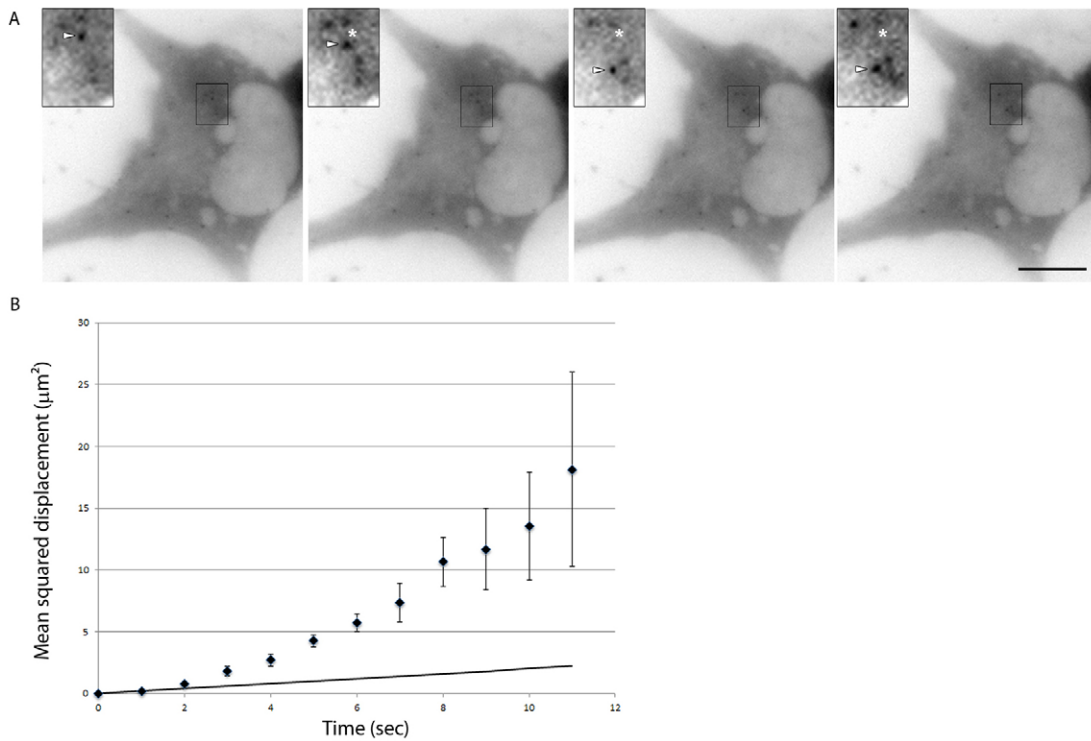


Fig. 6. SMIGs show directed movements. (A) MLN51 shows directed movement in the cytoplasm. HeLa cells were transfected with CFP–MLN51. After 24 hours, cells were observed for 5 minutes by using time-lapse video. Photographs of one cell were selected for this figure. Each panel is separated by 0.5 s. The insets show a region of interest indicated by the black box in the main image. In the insets, arrowheads indicate the position of the foci and asterisks indicate their positions at $t=0$. Scale bar: 10 μm . (B) Mean squared displacement calculation for SMIGs (dots). The graph represents the mean squared displacement as a function of time (\pm s.d.). The unbroken line represents the mean squared displacement for particles undergoing Brownian movements.

DISCUSSION

MLN51 is the only core EJC component that localizes mainly in the cytoplasm. In this study, we show for the first time that endogenous MLN51 is a component of P-bodies. It has been suggested that a small part of MLN51 is associated with polysomes (Degot et al., 2004). An interesting question is whether MLN51 localizes independently of the EJC or is only present in EJC-associated P-bodies. The absence of other core EJC components (eIF4A3, Magoh and Y14) from P-bodies (Chan et al., 2004; Chuang et al., 2013) favors the hypothesis of an independent mode of localization. Chuang et al. recently demonstrated that, in addition to its role in the EJC core, Y14 also has other important functions, and its overexpression leads to an increase in the number of P-bodies (Chuang et al., 2013). This Y14 action is opposite to that reported here for MLN51. Although we did not see that Y14 overexpression in HeLa cells had an effect on P-body numbers, both studies suggest that, following pioneer rounds of translation, several conformational changes might occur within the EJC core, thus allowing some of its factors to play additional roles in mRNA metabolism. However, it has to be noted that, as with Y14, the MLN51 region that is involved in non-EJC function is not the same as the one involved in its recruitment to the core complex ((Degot et al., 2004), this report). Moreover, we show that the effect of MLN51 overexpression on P-bodies can be reproduced when overexpressing a mutated MLN51 that is unable to bind to the EJC. This suggests that MLN51 can assemble on mRNAs independently of the EJC. Further studies will be necessary to elucidate the molecular mechanisms that allow them to perform these extra functions.

When overexpressed, MLN51 localizes in stress granules, but also mainly assembles in new and currently uncharacterized small cytoplasmic granules that we have named ‘small MLN51-induced granules’ (SMIGs). SMIGs contain poly(A)⁺ mRNA and show directed movements. SMIGs might be stress granule precursors, small P-bodies or an entirely new type of granule. Here, we show that SMIGs and stress granules differ in composition and kinetics. Using immunofluorescence, we could not detect a common P-body marker (such as Dcp1a, p54, Ge1 or Xrn1) in SMIGs. These observations favor the third hypothesis and suggest that these are a new type of RNA-containing granule. Other components of SMIGs are now under investigation. Interestingly, MLN51 is the human homolog of fly and mouse barentsz. Functional genetic screening has shown that barentsz is essential for *oskar* mRNA localization (van Eeden et al., 2001). Barentsz is also located in Staufen1 particles, which transport mRNAs along microtubules in the dendrites of mouse hippocampal neurons (Macchi et al., 2003). Dynamics studies have shown that to localize in a P-body a target must find its own way rather than relying on the active movement of a P-body to reach it (Aizer and Shav-Tal, 2008). It has also been reported that mRNA is required for cytoplasmic P-body maintenance (Cougot et al., 2004; Andrei et al., 2005; Ferraiuolo et al., 2005). Furthermore, a recent study showed that after nocodazole treatment, HIF-1 α mRNA, which is overexpressed in solid tumors, accumulates in P-bodies. It then associates with Ago2, a member of the miRNA pathway, thus leading to translational repression (Carbonaro et al., 2011). Finally, it has been recently shown that in

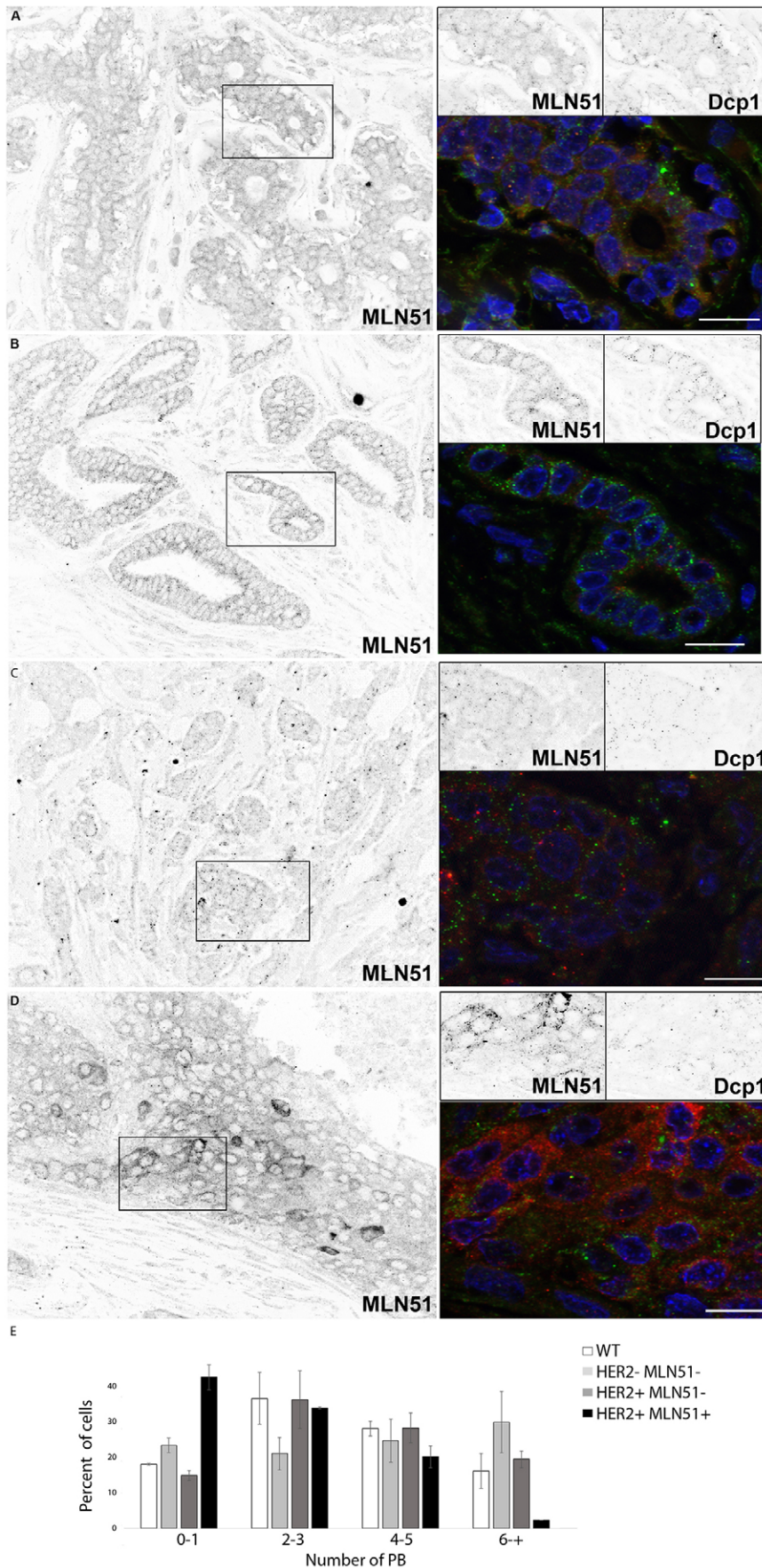


Fig. 7. The number of P-bodies is reduced in HER2⁺ breast cancer cells that overexpress MLN51. Detection of endogenous MLN51 by immunofluorescence using anti-MLN51 in (A) wild-type (WT) breast cells (patient P12/28 821), (B) HER2⁻/MLN51⁻ breast cancer cells (patient 207861), (C) HER2⁺/MLN51⁻ breast cancer cells (patient 20416E) and (D) HER2⁺/MLN51⁺ breast cancer cells (patient 204817). The insets represent the regions outlined in black in the main images. Insets show detection of MLN51 (upper left) and Dcp1a (upper right), as well as overlays where nuclei are stained with DAPI (blue). Scale bars: 20 μm (E) Distribution of the number of P-bodies (PB) per cell in HER2⁺/MLN51⁺ breast cancer cells (black), HER2⁺/MLN51⁻ breast cancer cells (dark gray), HER2⁻/MLN51⁻ breast cancer cells (light gray) or normal breast cells (white). For each, ten random fields were captured and P-bodies were counted on 1299, 1103, 910 and 128 cells, respectively. Data show the mean ± s.d.

rat brains, barentsz associates with mRNAs, translational regulators and factors involved in miRNA-mediated translational repression in RNA granules (Fritzsche et al., 2013). Here, we show that SMIGs induced by MLN51 overexpression lead to the disassembly of mammalian P-bodies in a microtubule-dependent manner. Thus, one attractive model would be that, when overexpressed, MLN51 is able to take some repressed mRNAs out of P-bodies, and that this causes P-body disassembly. Besides its EJC function, therefore, MLN51 would also act as a transport factor for certain repressed mRNAs, being involved in their recycling out of the P-body via the microtubule network. In such a model, SMIGs would be RNA transport granules that induce P-body disassembly by titrating cytoplasmic RNA out of these structures in a microtubule-dependent manner. Nocodazole treatment would thus trap the SMIGs in P-bodies, preventing overexpression of the SMIG-associated transcripts. A more complete characterization of SMIGs will help us to better understand their function.

Interestingly, MLN51 is overexpressed in malignant breast cancer cells (Tomasetto et al., 1995; Degot et al., 2002; Arriola et al., 2008). *MLN51* has been mapped to the q11–q21.3 region on the long arm of chromosome 17, a region also containing the *c-ErbB2* gene (Tomasetto et al., 1995). The *c-ErbB2* oncogene codes for the protein HER2, a tyrosine kinase belonging to the epidermal growth factor receptor family. Importantly, HER2 is overexpressed in ~30% of human breast cancers, where it must play a major role in pathogenesis, because its overproduction correlates with tumor chemo-resistance and poor patient prognosis (Klapper et al., 2000; Degot et al., 2002). As part of the HER2 or *ErbB2* amplicon, MLN51 is co-overexpressed in ~50% of HER2⁺ breast cancer cells (Degot et al., 2002; Arriola et al., 2008). Similar to what is observed in HeLa cells after MLN51 overexpression, here, we show that P-bodies are also disassembled in MLN51-overexpressing HER2⁺ breast cancer cells. Maturation of an miRNA subset is impaired in tumor cells (Thomson et al., 2006), and impairing the miRNA processing pathway promotes tumorigenesis (Kumar et al., 2007). One attractive model would be that overexpression of MLN51 in HER2⁺ breast cancer cells leads to deregulation of the mechanism of miRNA-mediated translational repression. A remaining question is whether the general miRNA translation repression pathway is perturbed in cancer cells, or whether this effect is restricted to certain subclasses of miRNA-repressed mRNAs localized in P-bodies. The first step then will be to identify which mRNAs can be trapped in and released from P-bodies following overexpression of MLN51.

PML nuclear bodies are an example of a non-membranous organelle that has been found to show cancer-associated changes. They are thought to have a link to cancer because of the observation that the PML–RAR α fusion protein disrupts nuclear bodies and contributes to leukemogenesis. Interestingly, treatment with arsenic or retinoic acid induces PML–RAR α degradation but also leads to nuclear body reassembly, thus suggesting that the presence or absence of nuclear bodies correlates with cell malignancy (de Thé et al., 2012). In this paper, we discuss P-body disassembly following overexpression of MLN51, a newly identified component of P-bodies. It is tempting to speculate that, as is the case for nuclear bodies, P-body status could mirror cell malignancy. We are currently investigating P-body status in cancer cells at various stages of tumorigenesis.

MATERIALS AND METHODS

Cell culture and transfections

HeLa cells were maintained in DMEM GlutaMAX (Invitrogen, Paisley, UK) containing 10% fetal calf serum (FCS) and 1 \times penicillin-streptomycin (Life Technologies). For transient transfection in six-well plates, 100–200 ng of plasmid DNA were transfected using Lipofectamine Plus Reagent (Invitrogen) following the manufacturer's protocol. For treatment with nocodazole (Sigma-Aldrich, St Louis, MO), the cells were treated with 30 μ M nocodazole for 2 hours at 24 hours after transfection. Cell sorting was performed on a FACSVantage SE option DiVa (BD Biosciences). Purity was >98%. Help for cell sorting was provided by C. Ebel (IGBMC).

Antibodies

To generate the anti-MLN51 rabbit polyclonal antibody, the synthetic peptide corresponding to residues 1–283 of the human MLN51 protein sequence was coupled to ovalbumin and injected into New Zealand rabbits. The rabbit anti-Dcp1a antibody was kindly supplied by Bertrand Séraphin (CNRS/IGBMC, Illkirch, France). The mouse anti-Dcp1a and anti-tubulin antibodies were from Abnova (Taipei City, Taiwan) and Sigma-Aldrich, respectively. Anti-MLN51 and -eIF4A3 antibodies were described previously (Degot et al., 2004; Dagueuet et al., 2012). Anti-TIA1 and anti-Ge1 were from Santa Cruz Biotechnology (Dallas, TX) and anti-DDX6, anti-ATXN2 were from INTERCHIM (Montluçon, France). Cy3- and FITC-conjugated goat anti-mouse-IgG or anti-rabbit-IgG antibodies were purchased from Jackson ImmunoResearch Laboratories (West Grove, PA).

Immunofluorescence

HeLa cells were seeded on glass coverslips and grown to 70% confluence. They were then washed with 1 \times PBS and fixed for 20 minutes at room temperature in 4% paraformaldehyde (PFA) in 1 \times PBS. After several washes with 1 \times PBS, cells were permeabilized with 0.1% Triton X-100 in 1 \times PBS for 10 minutes, then saturated for 30 minutes with 0.2% bovine serum albumin (BSA) in 1 \times PBS. After three washes with 1 \times PBS, cells were incubated for 1 hour at room temperature with the primary antibodies (1:1000). After another three washes with 1 \times PBS, cells were incubated for 1 hour with the appropriate Cy3- or FITC-conjugated secondary antibodies (1:1000). Cells were then washed and slides were mounted on Vectashield Medium with DAPI for nuclear counterstaining (Vector Laboratories, Burlingame, CA). Observations were made with an AxioImager Z1 upright microscope using Axiovision software (Zeiss, Oberkochen, Germany).

Fluorescence *in situ* hybridization

Poly(A)⁺ RNAs were detected by *in situ* hybridization (Bühler et al., 2002). Cells were grown on coverslips for 48 hours, fixed with 4% PFA for 30 minutes, then permeabilized overnight at 4°C with 70% ethanol. Cells were then rehydrated with 2 \times SSC containing 50% formamide, and hybridization was carried out with 300 ng Cy5-labeled oligo d(T) in 30% formamide in a humidified dark chamber at 37°C for 3 hours. After three washes with 2 \times SSC containing 30% formamide, the coverslips were subjected to standard immunofluorescence, mounted and analyzed as described above.

Immunofluorescence on HER2⁺ and normal breast cells

Paraffin-embedded tissue was cut into 4- μ m-thick sections, mounted on positively charged slides, then dried at 58°C for 60 minutes. Immunohistochemical staining was performed on the Discovery XT Automated IHC staining system (Ventana, Tucson, AZ). Following deparaffination with Ventana EZ Prep solution at 75°C for 8 minutes, antigen retrieval was performed at 95–100°C for 48 minutes using CC1, a proprietary Ventana Tris-based buffer solution. After rinsing, slides were incubated at 37°C for 60 minutes with a 1:50 dilution of rabbit anti-MLN51 and 1:50 mouse anti-Dcp1a. Detection was performed using Alexa-Fluor-555-conjugated goat anti-rabbit-IgG and the Alexa-Fluor-488-conjugated goat anti-mouse-IgG (both from Invitrogen) for 45 minutes at room temperature. DAPI staining was performed in

order to visualize the nuclei. Images were acquired on a Nikon Ni-E microscope and deconvoluted using the NIS-Elements AR software.

Immunohistochemistry

Paraffin-embedded tissue was cut into 4- μ m-thick sections, mounted on positively charged slides, then dried at 58°C for 60 minutes. Immunohistochemical staining was performed on the Discovery XT Automated IHC staining system using the Ventana DAB Map detection kit. Following deparaffination with Ventana EZ Prep solution at 75°C for 8 minutes, antigen retrieval was performed at 95–100°C for 48 minutes using Ventana CC1. Endogenous peroxidase was blocked with Inhibitor-D 3% H₂O₂ (Ventana) for 4 minutes at 37°C. For MLN51 staining, the slides were incubated after rinsing at 37°C for 60 minutes with a 1:100 dilution of rabbit anti-MLN51. Signal enhancement was performed using the Ventana DAB Map Kit. Biotinylated goat anti-rabbit-IgG (H⁺L) was used as the secondary antibody (Vector). For HER2 detection, slides were incubated at 37°C for 20 minutes with a 1:1000 dilution of polyclonal rabbit antibody against human HER2 (Dako, Glostrup, Denmark). Signal enhancement was performed using the UltraView Universal DAB (Ventana) and goat anti-rabbit-IgG HRP. Slides were then counterstained for 8 minutes and manually dehydrated before coverslips were added. Slides were treated with a Hamamatsu NanoZoomer 2.0-RS scanner and images were visualized with the NDP.view 1.2.47 software.

Live-cell imaging

peCFP-MLN51 (Degot et al., 2002; Degot et al., 2004) were transfected into HeLa cells. At 24 hours post-transfection, acquisition was performed on a Nikon TE200 widefield microscope (100 \times NA 1.45 objective) equipped with an EM-CCD camera (Cascade 512B, Roper Scientific). Z-stacks were captured every 0.5 s for 5 minutes. The Z-stacks were used to assemble movies using MetaMorph software (Molecular Devices, Sunnyvale, CA).

High-pressure freezing and freeze substitution

A cell slurry was made by resuspending HeLa cells in 20% BSA in DMEM. A 2- μ l drop of the sample was loaded onto a pre-heated, 0.5-mm-thick flat specimen carrier. This had gold-plated surfaces and a cavity diameter of 1.5 mm and depth of 0.2 mm (catalog number 16706898, Leica Microsystems AG, Wetzlar, Germany). Cells were frozen in a Leica EM PACT2 high-pressure freezer. Samples were transferred to an automatic freeze-substitution system (Leica EM AFS2) equipped with an automatic reagent handling system (EM FSP), then placed in the precooled –90°C substitution solution. Cells were freeze-substituted in acetone containing 0.1% uranyl acetate at –90°C for 60 hours. The temperature was then increased to –50°C at a rate of 3°C per hour, and samples were kept at this temperature for 24 hours. The samples were then washed once with acetone and three times with 100% ethanol at –50°C. Samples were infiltrated with resin/100% ethanol mixtures by raising the volume-to-volume proportion of Lowicryl HM20 as follows: 2 hours at 25%, 2 hours at 50%, overnight at 75% and, finally, 1 hour (four times) at 100%. Finally, polymerization was carried out at –50°C for 48 hours and at 20°C for 48 hours. Ultrathin 90–110 nm sections were collected on 300-mesh nickel grids.

Immunoelectron microscopy

Lowicryl HM20-embedded thin sections were first blocked with 1% serum albumin in 100 mM pH 7.4 phosphate buffer for 2.5 hours, then allowed to react for 2 hours with primary antibody diluted in blocking buffer. The dilutions were 1:250 for rabbit and mouse anti-Dcp1a, and for rabbit anti-MLN51. Following four 10-minute washes with blocking buffer, and one wash in 100 mM Tris-HCl pH 7.4 buffer containing 1% serum albumin, grids were incubated for 1 hour with the goat anti-rabbit-IgG or anti-mouse IgG antibody coupled to gold particles at a dilution of 1:40 (Delta Microscopies, Agyesvives, France). After subsequent washes with the same buffer, grids were fixed with 2.5% glutaraldehyde and contrasted for 1.5 hours in 5% uranyl acetate.

Double immuno-detections consisted of repeating two single immuno-detections in a row: a first detection using rabbit anti-MLN51 revealed with goat anti-rabbit IgG conjugated to 6-nm gold particles, and a second detection using mouse anti-Dcp1a revealed with goat anti-mouse IgG conjugated to 15-nm gold particles.

Human patient samples

Human patient samples were analyzed as described above. The study cohort was made up of ten patients and included two samples of non-malignant breast cells, three HER2[–] and five HER2⁺ breast cancer samples. This study was approved by the institutional boards of the Centre de Ressources Biologiques Santé de Rennes.

Acknowledgements

We are grateful to Bruno Turlin, Florence Godey and Mireille Dugast (Centre de Ressources Biologiques Santé de Rennes, France) and Jean Levêque (Département de Gynécologie et d'Obstétrique, Centre Hospitalier Universitaire de Rennes, France) for invaluable help with the clinical part of the present investigation. We would like to thank Bertrand Séraphin (Institut Génétique Biologie Moléculaire Cellulaire, Strasbourg, France) for providing us with the anti-Dcp1a antibody and to Juliana Berland for insightful comments on the manuscript. Electron microscopy experiments were processed at the Microscopy Rennes Imaging Center (MRic) facilities (<http://microscopie.univ-rennes1.fr/>).

Competing interests

The authors declare no competing interests.

Author contributions

N.C. conceived and performed the experiments; analyzed data and wrote the manuscript. E.D. performed experiments with immunofluorescence; A.B. performed experiments with immunofluorescence, before and during the revision process; A.C. performed experiments with high pressure freezing and freeze substitution; D.T. performed experiments with immunoelectron microscopy; P.B. and A.F. performed experiments with human patient samples; F.G. designed and selected the study cohort; E.B. conceived experiments and performed videomicroscopy data analysis; C.T. conceived experiments, performed immunofluorescence and W.B. experiments during the revision process; R.G. directed the project and analyzed data. N.C. wrote the manuscript with advice and comments from the other authors. All the authors contributed to the design and interpretation of experiments.

Funding

This work was supported by the French National Agency [grant numbers ANR-08JJC-0027-01 and ANR-09-MIE]; the Institut Universitaire de France; and the Ligue Nationale Contre le Cancer. E.D. had a fellowship from the Fondation pour la Recherche Médicale (FRM). Funds to C.T. were from The Ligue Nationale Contre Le Cancer (CCIR-GE).

Supplementary material

Supplementary material available online at <http://jcs.biologists.org/lookup/suppl/doi:10.1242/jcs.154500/-DC1>

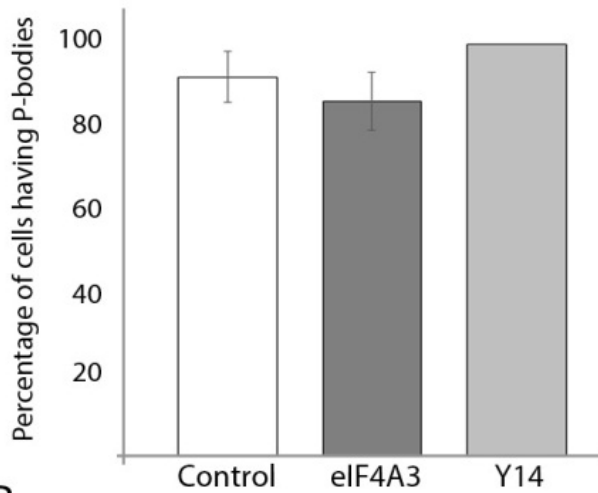
References

- Aizer, A. and Shav-Tal, Y. (2008). Intracellular trafficking and dynamics of P bodies. *Prion* **2**, 131–134.
- Aizer, A., Brody, Y., Ler, L. W., Sonenberg, N., Singer, R. H. and Shav-Tal, Y. (2008). The dynamics of mammalian P body transport, assembly, and disassembly in vivo. *Mol. Biol. Cell* **19**, 4154–4166.
- Anderson, P. and Kedersha, N. (2006). RNA granules. *J. Cell Biol.* **172**, 803–808.
- Andrei, M. A., Ingelfinger, D., Heintzmann, R., Achsel, T., Rivera-Pomar, R. and Lührmann, R. (2005). A role for eIF4E and eIF4E-transporter in targeting mRNPs to mammalian processing bodies. *RNA* **11**, 717–727.
- Arriola, E., Marchio, C., Tan, D. S., Drury, S. C., Lambros, M. B., Natrajan, R., Rodriguez-Pinilla, S. M., Mackay, A., Tamber, N., Fenwick, K. et al. (2008). Genomic analysis of the HER2/TOP2A amplicon in breast cancer and breast cancer cell lines. *Lab. Invest.* **88**, 491–503.
- Baguet, A., Degot, S., Cougot, N., Bertrand, E., Chenard, M. P., Wendling, C., Kessler, P., Le Hir, H., Rio, M. C. and Tomasetto, C. (2007). The exon-junction-complex-component metastatic lymph node 51 functions in stress-granule assembly. *J. Cell Sci.* **120**, 2774–2784.
- Balagopal, V. and Parker, R. (2009). Polysomes, P bodies and stress granules: states and fates of eukaryotic mRNAs. *Curr. Opin. Cell Biol.* **21**, 403–408.
- Bailly, L., Marchadier, B., Baguet, A., Tomasetto, C., Séraphin, B. and Le Hir, H. (2005). The exon junction core complex is locked onto RNA by inhibition of eIF4AIII ATPase activity. *Nat. Struct. Mol. Biol.* **12**, 861–869.

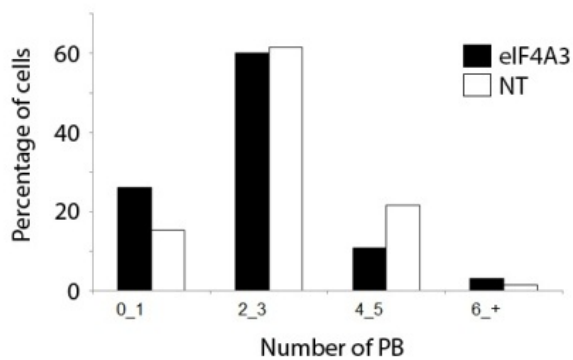
- Bièche, I., Tomasetto, C., Régnier, C. H., Moog-Lutz, C., Rio, M. C. and Lidereau, R. (1996). Two distinct amplified regions at 17q11-q21 involved in human primary breast cancer. *Cancer Res.* **56**, 3886–3890.
- Buchan, J. R. and Parker, R. (2009). Eukaryotic stress granules: the ins and outs of translation. *Mol. Cell* **36**, 932–941.
- Bühler, M., Wilkinson, M. F. and Mühlemann, O. (2002). Intranuclear degradation of nonsense codon-containing mRNA. *EMBO Rep.* **3**, 646–651.
- Carbonaro, M., O'Brate, A. and Giannakakou, P. (2011). Microtubule disruption targets HIF-1 α mRNA to cytoplasmic P-bodies for translational repression. *J. Cell Biol.* **192**, 83–99.
- Chan, C. C., Dostie, J., Diem, M. D., Feng, W., Mann, M., Rappsilber, J. and Dreyfuss, G. (2004). eIF4A3 is a novel component of the exon junction complex. *RNA* **10**, 200–209.
- Chazal, P. E., Daguene, E., Wendling, C., Ulryck, N., Tomasetto, C., Sargueil, B. and Le Hir, H. (2013). EJC core component MLN51 interacts with eIF3 and activates translation. *Proc. Natl. Acad. Sci. USA* **110**, 5903–5908.
- Chuang, T. W., Chang, W. L., Lee, K. M. and Tarn, W. Y. (2013). The RNA-binding protein Y14 inhibits mRNA decapping and modulates processing body formation. *Mol. Biol. Cell* **24**, 1–13.
- Cougot, N., Babajko, S. and Séraphin, B. (2004). Cytoplasmic foci are sites of mRNA decay in human cells. *J. Cell Biol.* **165**, 31–40.
- Cougot, N., Cavalier, A., Thomas, D. and Gillet, R. (2012). The dual organization of P-bodies revealed by immunoelectron microscopy and electron tomography. *J. Mol. Biol.* **420**, 17–28.
- Cougot, N., Molza, A. E., Giudice, E., Cavalier, A., Thomas, D. and Gillet, R. (2013). Structural organization of the polysomes adjacent to mammalian processing bodies (P-bodies). *RNA Biol.* **10**, 314–320.
- Daguene, E., Baguet, A., Degot, S., Schmidt, U., Alpy, F., Wendling, C., Spiegelhalter, C., Kessler, P., Rio, M. C., Le Hir, H. et al. (2012). Perispeckles are major assembly sites for the exon junction core complex. *Mol. Biol. Cell* **23**, 1765–1782.
- de Thé, H., Le Bras, M. and Lallemand-Breitenbach, V. (2012). The cell biology of disease: Acute promyelocytic leukemia, arsenic, and PML bodies. *J. Cell Biol.* **198**, 11–21.
- Degot, S., Régnier, C. H., Wendling, C., Chenard, M. P., Rio, M. C. and Tomasetto, C. (2002). Metastatic Lymph Node 51, a novel nucleo-cytoplasmic protein overexpressed in breast cancer. *Oncogene* **21**, 4422–4434.
- Degot, S., Le Hir, H., Alpy, F., Kedinger, V., Stoll, I., Wendling, C., Séraphin, B., Rio, M. C. and Tomasetto, C. (2004). Association of the breast cancer protein MLN51 with the exon junction complex via its speckle localizer and RNA binding module. *J. Biol. Chem.* **279**, 33702–33715.
- Eulalio, A., Behm-Ansmant, I., Schweizer, D. and Izaurralde, E. (2007). P-body formation is a consequence, not the cause, of RNA-mediated gene silencing. *Mol. Cell Biol.* **27**, 3970–3981.
- Eystathiou, T., Chan, E. K., Tenenbaum, S. A., Keene, J. D., Griffith, K. and Fritzler, M. J. (2002). A phosphorylated cytoplasmic autoantigen, GW182, associates with a unique population of human mRNAs within novel cytoplasmic speckles. *Mol. Biol. Cell* **13**, 1338–1351.
- Ferraiuolo, M. A., Basak, S., Dostie, J., Murray, E. L., Schoenberg, D. R. and Sonenberg, N. (2005). A role for the eIF4E-binding protein 4E-T in P-body formation and mRNA decay. *J. Cell Biol.* **170**, 913–924.
- Fritzsche, R., Karra, D., Bennett, K. L., Ang, F. Y., Heraud-Farlow, J. E., Tolino, M., Doyle, M., Bauer, K. E., Thomas, S., Planyavsky, M. et al. (2013). Interactome of two diverse RNA granules links mRNA localization to translational repression in neurons. *Cell Reports* **5**, 1749–1762.
- Gehring, N. H., Kunz, J. B., Neu-Yilik, G., Breit, S., Viegas, M. H., Hentze, M. W. and Kulozik, A. E. (2005). Exon-junction complex components specify distinct routes of nonsense-mediated mRNA decay with differential cofactor requirements. *Mol. Cell* **20**, 65–75.
- Ivanov, P. A., Chudinova, E. M. and Nadezhdina, E. S. (2003). Disruption of microtubules inhibits cytoplasmic ribonucleoprotein stress granule formation. *Exp. Cell Res.* **290**, 227–233.
- Kedersha, N. and Anderson, P. (2007). Mammalian stress granules and processing bodies. *Methods Enzymol.* **431**, 61–81.
- Klapper, L. N., Kirschbaum, M. H., Sela, M. and Yarden, Y. (2000). Biochemical and clinical implications of the ErbB/HER signaling network of growth factor receptors. *Adv. Cancer Res.* **77**, 25–79.
- Kumar, M. S., Lu, J., Mercer, K. L., Golub, T. R. and Jacks, T. (2007). Impaired microRNA processing enhances cellular transformation and tumorigenesis. *Nat. Genet.* **39**, 673–677.
- Macchi, P., Kroening, S., Palacios, I. M., Baldassa, S., Grunewald, B., Ambrosino, C., Goetze, B., Lupas, A., St Johnston, D. and Kiebler, M. (2003). Barentsz, a new component of the Staufen-containing ribonucleoprotein particles in mammalian cells, interacts with Staufen in an RNA-dependent manner. *J. Neurosci.* **23**, 5778–5788.
- Mollet, S., Cougot, N., Wilczynska, A., Dautry, F., Kress, M., Bertrand, E. and Weil, D. (2008). Translationally repressed mRNA transiently cycles through stress granules during stress. *Mol. Biol. Cell* **19**, 4469–4479.
- Nott, A., Le Hir, H. and Moore, M. J. (2004). Splicing enhances translation in mammalian cells: an additional function of the exon junction complex. *Genes Dev.* **18**, 210–222.
- Palacios, I. M., Gatfield, D., St Johnston, D. and Izaurralde, E. (2004). An eIF4AIII-containing complex required for mRNA localization and nonsense-mediated mRNA decay. *Nature* **427**, 753–757.
- Parker, R. and Sheth, U. (2007). P bodies and the control of mRNA translation and degradation. *Mol. Cell* **25**, 635–646.
- Pillai, R. S., Bhattacharyya, S. N., Artus, C. G., Zoller, T., Cougot, N., Basyuk, E., Bertrand, E. and Filipowicz, W. (2005). Inhibition of translational initiation by Let-7 MicroRNA in human cells. *Science* **309**, 1573–1576.
- Sheth, U. and Parker, R. (2003). Decapping and decay of messenger RNA occur in cytoplasmic processing bodies. *Science* **300**, 805–808.
- Sweet, T. J., Boyer, B., Hu, W., Baker, K. E. and Collier, J. (2007). Microtubule disruption stimulates P-body formation. *RNA* **13**, 493–502.
- Tange, T. O., Shibuya, T., Jurica, M. S. and Moore, M. J. (2005). Biochemical analysis of the EJC reveals two new factors and a stable tetrameric protein core. *RNA* **11**, 1869–1883.
- Thomson, J. M., Newman, M., Parker, J. S., Morin-Kensicki, E. M., Wright, T. and Hammond, S. M. (2006). Extensive post-transcriptional regulation of microRNAs and its implications for cancer. *Genes Dev.* **20**, 2202–2207.
- Tomasetto, C., Régnier, C., Moog-Lutz, C., Mattei, M. G., Chenard, M. P., Lidereau, R., Basset, P. and Rio, M. C. (1995). Identification of four novel human genes amplified and overexpressed in breast carcinoma and localized to the q11-q21.3 region of chromosome 17. *Genomics* **28**, 367–376.
- van Eeden, F. J., Palacios, I. M., Petronczki, M., Weston, M. J. and St Johnston, D. (2001). Barentsz is essential for the posterior localization of oskar mRNA and colocalizes with it to the posterior pole. *J. Cell Biol.* **154**, 511–524.

SUPPLEMENTARY FIGURES

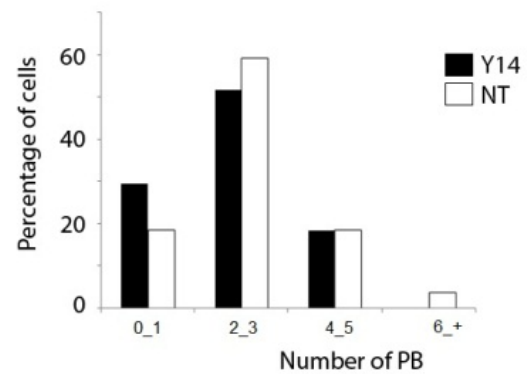
A



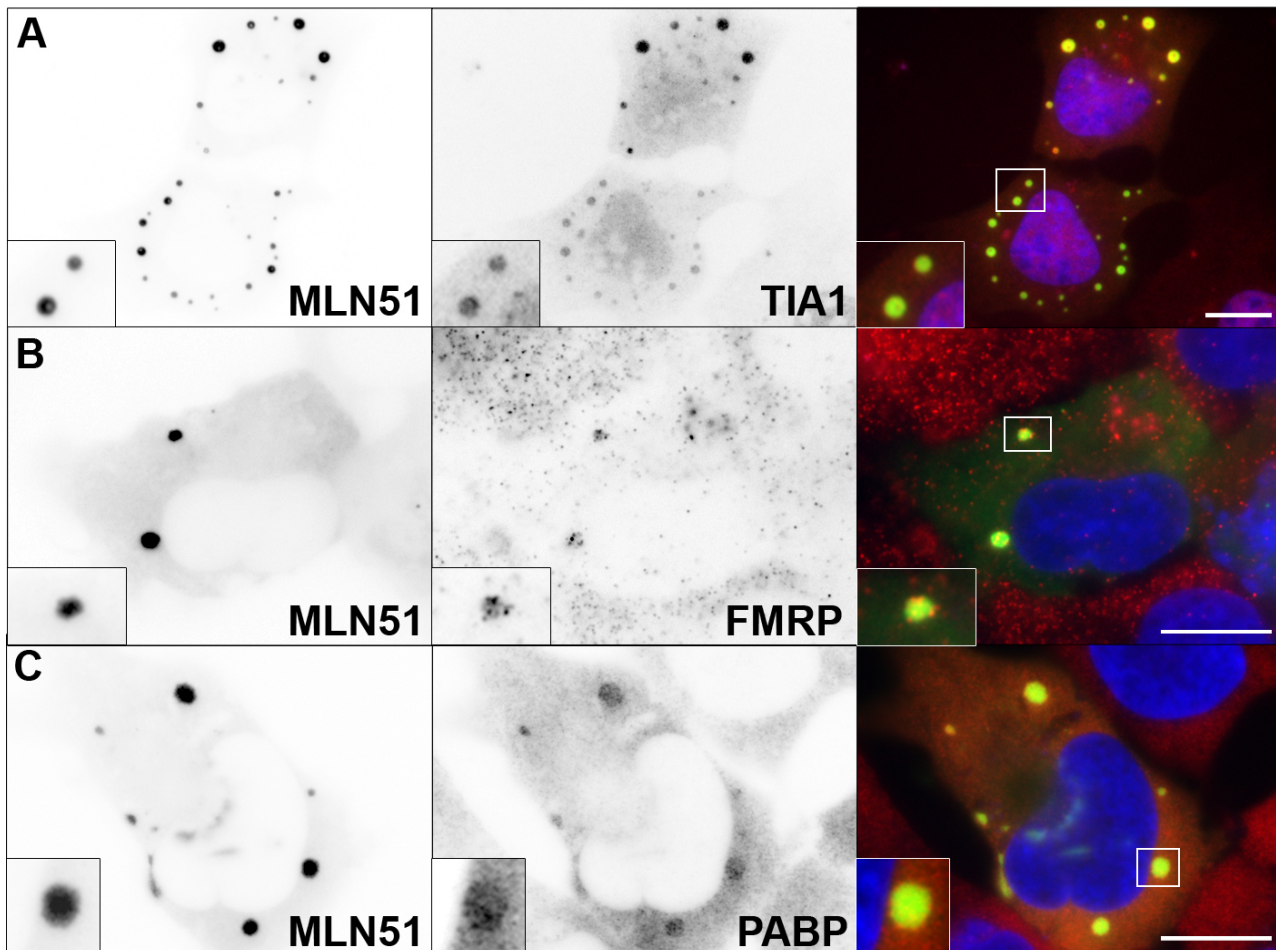
B



C

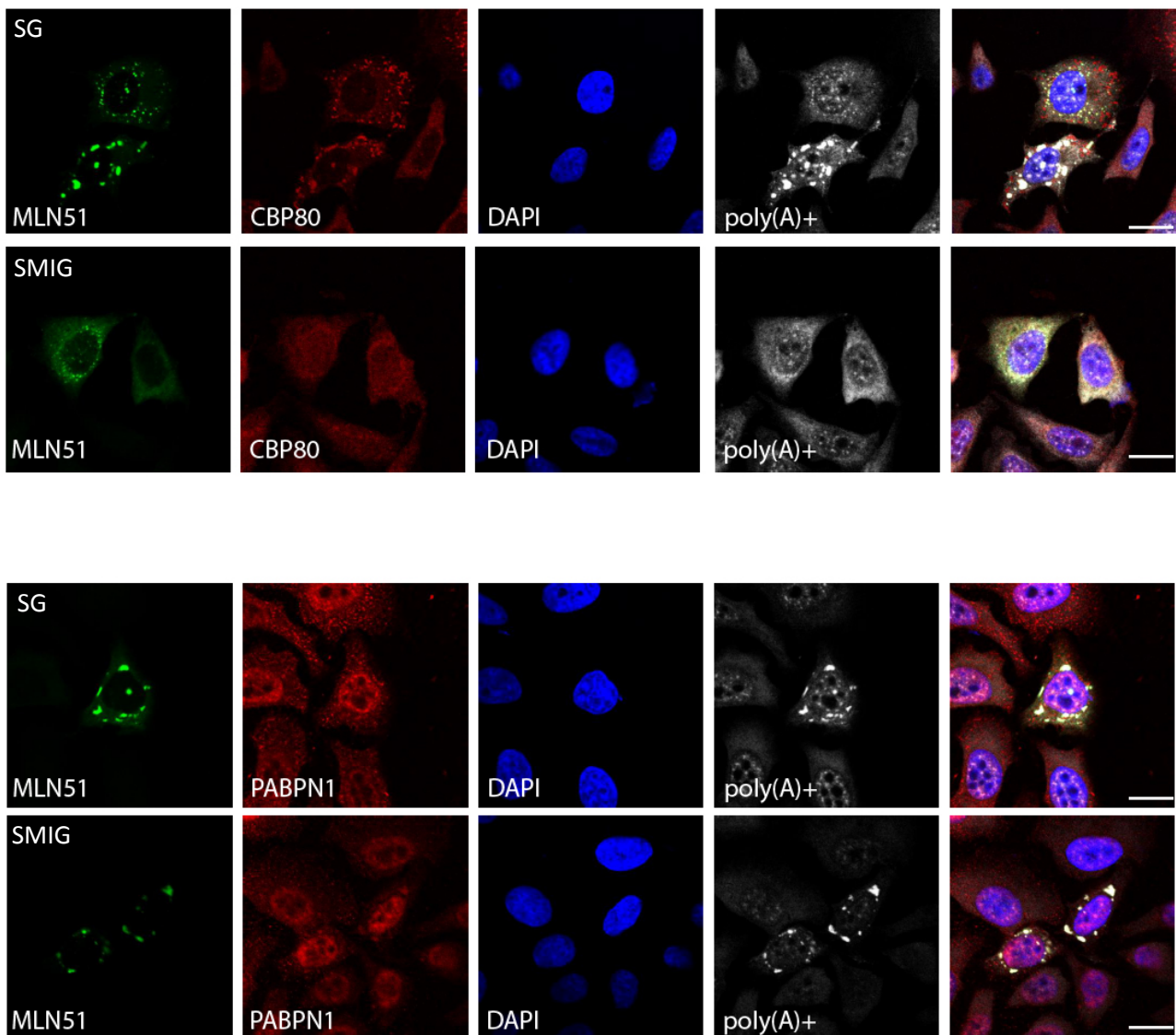


Supplementary Figure 1: Overexpression of other EJC core components do not lead to disassembly of PB. Graph of the percentage of cells having at least one P-body following overexpression of CFP fusion of eIF4A3 or Y14. Each experiment corresponds to at least 40 cells captured on 11 different fields. B and C: Distribution of the number of PBs per cell following overexpression of CFP-eIF4A3 (B) or CFP-Y14 (C). NT, untransfected cells. Data represent the mean of 3 independent experiments, the error bar representing standard deviation.



Supplementary Figure 2: The large cytoplasmic granules observed upon expression of the CFP-MLN51 C-terminal fragment (CFP-MLN51Ct) are stress granules.

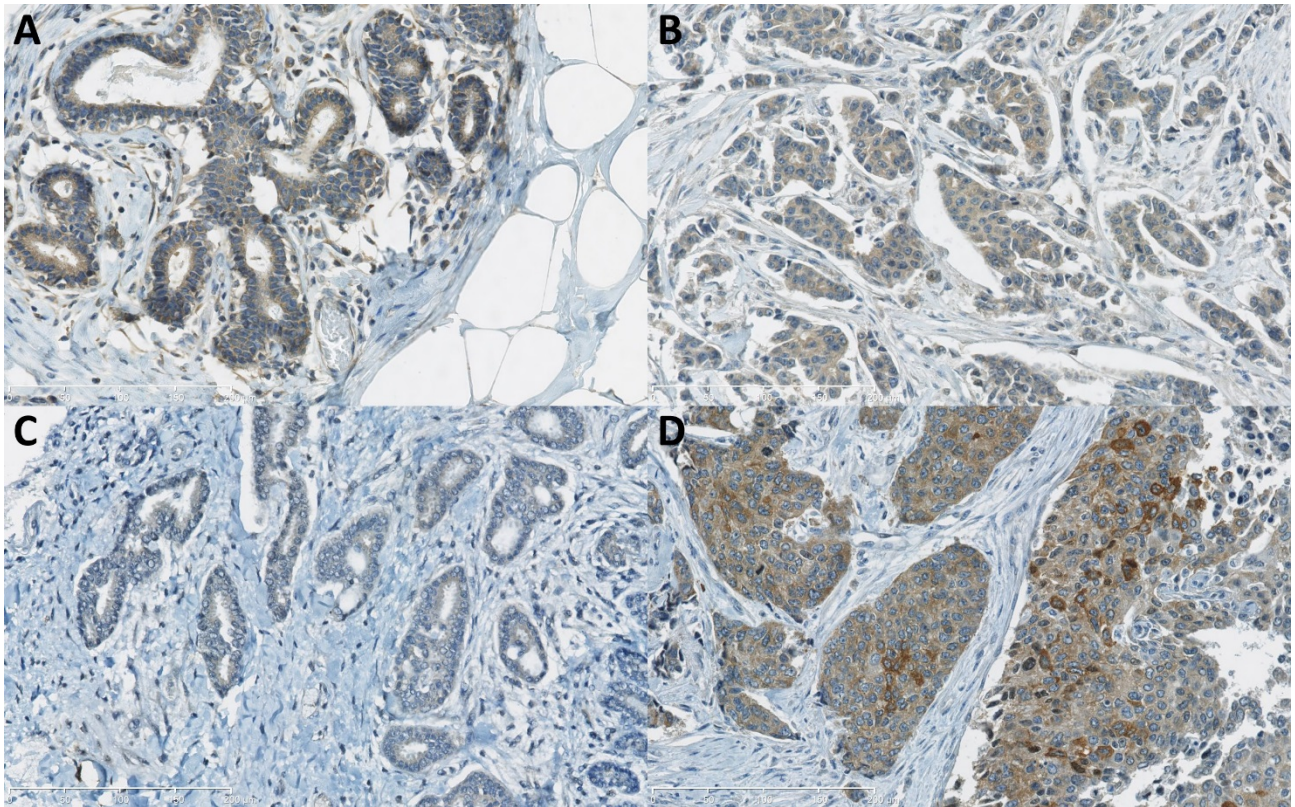
Cells were transfected with CFP-MLN51Ct (left panels, green in right panels). SGs (central panels, red in right panels) were then immuno-detected with the following antibodies: anti-TIA1 (A), anti-FMRP (B), or anti-PABP (C). Right panels show overlays with DAPI-stained nuclei (blue). Scale bar: 10 μ m. Insets show granule enlargements.



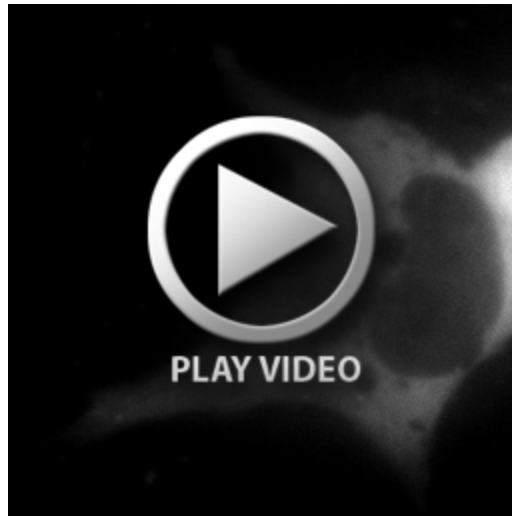
Supplementary Figure 3: co-staining experiments of MLN51 with the nuclear cap-binding protein CBP80 and with the nuclear form of PABP.

CFP-MLN51 (left panels, green on right panels) was transfected in HeLa cells. 24 hours following transfection, poly(A)⁺ mRNA (fourth panels, white on right panels) were detected by fluorescence in situ hybridization with a Cy3-labelled oligod(T) probe.

CBP80 or PABPN1 (second panels, red on right panels) were detected with anti-CBP80 (top) or anti-PABPN1 (bottom) antibodies, respectively. (Top) SG contain poly(A)⁺ mRNA and CBP80; SG contain PABPN1 and poly(A)⁺ mRNAs. SMIG contain poly(A)⁺ mRNAs but not CBP80. (Bottom) SMIG contain poly(A)⁺ mRNA but no PABPN1. Scale bar: 10μm.



Supplementary Figure 4: Immunohistochemical analysis of MLN51 subcellular localization in breast cells.(A) breast cells (patient P12/28 821); (B) HER2-negative breast cancer cells (patient 207861); (C) HER2-positive cancer cells not overexpressing MLN51 (patient 20416E); and (D) HER2-positive cancer cells overexpressing MLN51 (patient 204817).



Movie 1. CFP-MLN51 foci in U2OS transfected cells. Duration: 5 minutes. Interval: 1 second.